

Received January 18, 2022, accepted February 8, 2022, date of publication February 17, 2022, date of current version March 9, 2022.

Digital Object Identifier 10.1109/ACCESS.2022.3152534

Cellular Base Station Imaging for UAV Detection

PAN CAO 

School of Physics, Engineering and Computer Science, University of Hertfordshire, Herts AL10 9AB, U.K.

e-mail: p.cao@herts.ac.uk

ABSTRACT As the use of unmanned aerial vehicles (UAVs) is greatly increasing, there is an emerging threat of using UAVs in infrastructure/cyber-attacks and data-eavesdropping. From the safety and security perspective, it is a timely need to build an air surveillance system that enables a seamless detection function for low-and-middle altitude flying targets. However, it is unrealistic to widely deploy classical radar stations due to the astronomical cost. Rethinking the role of cellular mobile communication networks, we desire to add a “vision-like” capability to the widely deployed outdoor cellular base stations (BSs) to realize joint imaging and communication (JIAC) simultaneously through sharing the existing cellular communication infrastructure and spectrum. In this work, it is for the first time to systematically study and demonstrate the concept of cellular base station imaging for UAV detection, which allows a cellular BS to work like an inverse synthetic-aperture radar (ISAR) besides communication. Firstly, we provide the JIAC transmission signalling and systematic operation mechanism. Secondly, the feasibility of JIAC is investigated and analysed to support the idea of cellular base station imaging. Finally, numerical simulation evaluates the imaging performance of three typical types of cellular BSs operating at 900 MHz, 3.5 GHz and 28 GHz, respectively, which implies that cellular BS imaging works for UAV detection! Furthermore, the radar imaging function, as a new by-product, requires only a very little change to the current orthogonal frequency-division multiplexing (OFDM) communication signalling and has nearly no influence on the current communication operation and performance.

INDEX TERMS Cellular mobile communication, joint imaging and communication (JIAC), high resolution radar imaging, unmanned aerial vehicles (UAVs) detection.

I. INTRODUCTION

The development of low-and-middle altitude unmanned aerial vehicles (UAVs) has attracted greatly increasing attention from both academia and industry, due to its benefits in flexible mobility, low cost and easy operation compared to conventional ground carriers and manned aircrafts. This leads to a host of different applications of UAVs to both aerial and ground missions such as product deliveries, agriculture, policing and surveillance, infrastructure inspections, disaster emergencies and UAV-assisted communication networks [1]–[3]. However, as a double-edge sword, the increasing use of UAVs could become one of the biggest emerging threats to the security and safety, e.g., invasion of privacy, unauthorised aerial surveillance & data collection, collisions with aircraft, and even terrorist attack, when they fall into the wrong hands. One fresh instance is that two explosive-laden drones crashed into the Indian Air Force station at Jammu in June 2021. Another notable case is that more than 140,000 passengers

and 1,000 flights were affected by the malicious drone attack at Gatwick Airport near London in December 2018. Therefore, there is a timely need to build an early-warning air surveillance system to track and identify the UAVs.

Radar is a sensing system that utilises radio frequency waves to sense targets in day/night all-weather conditions. If classical air-defence radar systems, e.g., military radar, are utilised to detect small UAVs, yet it seems like to fire cannons to kill mosquitoes. Furthermore, it is also unrealistic to widely deploy classical radar stations, e.g., military radars, so as to provide seamless coverage due to the astronomical cost. As a result, UAVs can easily defeat conventional air-defence system due to its limited coverage as the aforementioned examples.

Cellular mobile networks have now been developed for 40 years from the first generation (1G) to the fifth generation (5G) that aims to provide seamless service coverage for massive mobile subscribers [4]. As typical cellular mobile networks only focus on the functions of “speaking” (transmitting signal) and “listening” (receiving signal), it is motivated to have a rethink and explore a new “vision-like”

The associate editor coordinating the review of this manuscript and approving it for publication was Yafei Hou .

function. A question has arisen - Is it possible to utilise the existing widely deployed cellular base stations to "see" flying targets but meanwhile without disrupting communication operation and performance? From a scientific perspective, this question might be realistic based on the following facts: 1) Wireless communication and radar sensing, both based on radio frequency waves, have similar hardware structure and system components in both baseband and RF ends, thereby allowing them to share most of the hardware and software; 2) Cellular bases stations are equipped with multiple antennas, even large scale antennas (tens or even hundreds antennas) in 5G, to generate large-gain directional beams, which can be used to combat the path loss for both communication and radar sensing; 3) Cellular base stations occupy large transmission spectrum, e.g., 20-100 MHz or even up to 400 MHz bands for sub-6 GHz by using carrier aggregation and 400 MHz - 2 GHz bands for for unlicensed millimetre waves (mm-waves), e.g., mm-wave signalling used for target detection [5], [6]. Wide transmission bands lead to both high data rate in communication and high range resolution in radar sensing.

Recently increasing research effort has been made on the study of the integration of sensing and communication (ISAC) that is recognized as an emerging feature in future beyond 5G and the sixth generation (6G) wireless systems [7]–[13]. Some recent research focuses on transceiver design in the radar-communication spectrum and infrastructure sharing scenarios, to realize the joint communication and radar operation mainly through beamforming and frame structure design [14], [15]; Some other work consider the waveform design [16]–[20] and joint radar-communication resource allocation [21]–[23] to optimize the trade-off between communication and radar performance in the ISAC systems. The above two classes of work study the ISAC mainly from the perspective of the physical layer signal processing and optimization, e.g., beamforming and signalling strategy design, to properly balance the radar-communication resource sharing. A different class of ISAC research is to utilize the existing wireless communication signals, e.g., WiFi/LiFi signals, to realize some sensing functions, which is like the by-product of wireless communication. In particular, active localization is a widely applied important way to estimate the receiver's position through actively measuring the signals' characteristics, e.g., the time of arrival (ToA), angle of arrival (AoA) or received signal strength (RSS), at the receiver from the access points [24]–[26]. Passive positioning and sensing is to detect target's (neither the transmitter nor receiver) position/movement features through observing and analysing the changes (e.g., micro Doppler frequency shift) of wireless channel state information, because the target's different location and movement, as a part of wireless propagation environment, have different influence on the wireless propagation channel state [27]. The performance of localization and passive sensing heavily rely on deployment and layout of the access points and receivers. There are also some excellent effort has been made on using communication signals to

realize radar imaging, for example, using WiFi signalling to detect human's movement and activities behind the wall based on ISAR technology [28], and the feasibility and limits have been analysed in [29]. In [30], the outdoor static environment is imaged by using cellular communication base stations based on synthetic-aperture radar (SAR) technology, and the potential of ISAR based imaging is also mentioned but lack of systematic study and demonstration.

In this work, it is for the first time to systematically study and demonstrate the concept of cellular base station imaging that allows an outdoor cellular base station to work like an ISAR to "see" flying targets, but meanwhile at nearly no extra cost of the current cellular mobile communication function and performance. From a systematic study point of view, we firstly provide the signalling strategy and operation mechanism for a cellular base station to realize JIAC. Then, the feasibility of cellular base station imaging is investigated and analysed based on the radar equation. The feasibility study provides a suggestion on the ability of cellular base station detection and imaging for different flying targets based on different types of cellular base stations. Finally, numerical simulations evaluate the imaging performance of cellular base stations operating at 900 MHz, 3.5 GHz and 28 GHz, respectively. The one-dimensional (1D) high resolution range profiles (HRRPs) and two-dimensional (2D) images are generated for the flying targets with different size and range, which verify the feasibility analysis of cellular base station imaging.

The outline of the paper is organized to address the above contributions on cellular base station imaging - its concept, JIAC signalling strategy and radar imaging technology in Section II, the feasibility study in Section III, simulation results in Section IV, and finally concluded in Section V, respectively.

II. CONCEPT, SIGNALLING STRATEGY AND IMAGING TECHNOLOGY

Consider a typical cellular base station equipped with multiple antennas that operates at spectrum band (f_c, B) in the downlink, where f_c and B denote the carrier frequency and the spectrum bandwidth both in Hertz (Hz). Based on this typical cellular base station system model, this section provides the concept, signalling strategy and imaging technology for the base station to allow the joint radar imaging and communication.

A. CONCEPT

Here, we introduce the concept of cellular base station imaging - integration the "vision-like" radar imaging functionality into cellular base stations to allow radar imaging for moving targets besides conventional communication simultaneously. With this concept, a base station can not only speak to and hear from mobile users as normal but also meanwhile can see moving targets. Cellular base station imaging enhances the functionality and capability of a base station in a different dimension. In principle, the cellular base station imaging can

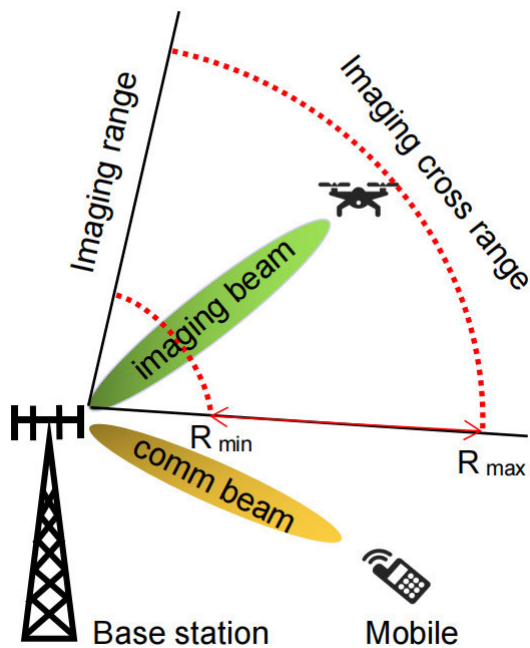


FIGURE 1. Cellular base station imaging system and concept.

be applied to both aerial and ground moving targets, e.g., vehicles. In this work, the illustration focus is given on flying targets, e.g., UAVs.

As illustrated in Fig.1, a cellular base station, usually deploy on the top of a tower or roof of the tall building, has an additional aerial radar sensing area targeting the flying objectives, besides the conventional mobile communication service mainly supporting ground mobile users. The joint of sensing and communication is based on the sharing of both infrastructure and spectrum. As the mobile communication function is little influenced by the new radar imaging function, the focus of the work is given on realizing the cellular base station imaging function. The effective imaging area ranging from a minimum distance R_{min} to the maximum distance R_{max} and a predefined angular range to cover the cross range dimension, which forms a three-dimensional (3D) effective monitoring space shaped-like a doughnut. The multi-antenna base station allows to generate directional beams pointing to mobile users and flying targets, respectively, in a space division multiple access manner and possibly also in different time sequence.

To implement of the radar sensing function, the base station runs exhaustive beam scanning periodically to searching potential targets, which can utilise off-line generated beam codebook as the beam swapping in beam training stage in mm-wave communication. Once the direction of interest is determined, for example where some unexpected echoes come, the base station starts to send out radar imaging signals pointing to the direction of interest for the target imaging and further recognition.

Regarding the clutter and interference in radar sensing, it is worth noting that flying targets experience much less or even ignorable clutter compared to ground targets. Even when

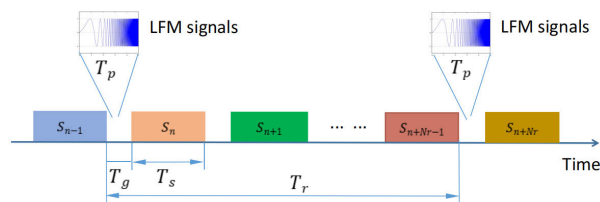


FIGURE 2. Cellular base station imaging OFDM based signalling strategy.

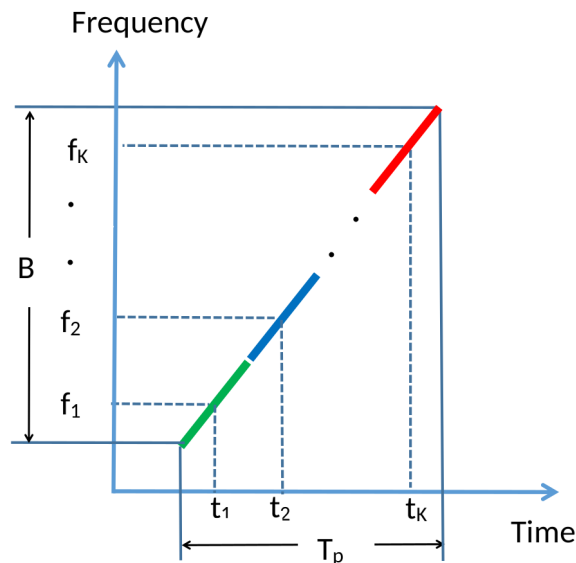


FIGURE 3. Cellular base station imaging OFDM based LFM signals.

there exist severe clutter and interference, e.g., multipath reflections by buildings and trees, they can still be mitigated by designing radar sensing beams to nullify the major clutter and interference directions that can be determined by estimating long-term static sensing channel in advance.

The detailed radar signalling strategy will be described in the following part.

B. SIGNALLING STRATEGY

Orthogonal frequency division multiplexing (OFDM) utilizes multiple carriers to transmit data in parallel, which forms the basic signal format in 4G/5G mobile communications. In this work, OFDM downlink signalling transmission is considered at cellular base stations.

As shown in Fig.2, the cellular base station transmits OFDM symbols $S_{n-1}, S_n, \dots, S_{n+N_r}$ sequentially in the downlink, where T_s and T_g denote the OFDM symbol duration and guard interval. The guard interval is utilised to separate the two adjacent OFDM symbols in order to eliminate inter-symbol interference. In order not to influence the OFDM symbols' transmission, we propose to insert radar imaging signals into some (not all) OFDM guard intervals that depends on the pulse repeat interval T_r , i.e., the radar sensing pulse signal is transmitted every T_r second. The radar imaging employs linear frequency modulated (LFM)

signal – chirp signal, which is defined as a radar pulse that spans within the time interval $T_{p,k}$ (with central time t_k) and the frequency range $[f_k - B_k/2, f_k + B_k/2]$ for the k -th carrier, where f_k and B_k denote the carrier frequency and bandwidth for the k -th carrier. When these LFM signals for the carriers are set as shown in Fig.3, they can be easily aggregated to a large LFM signal spanning within the total frequency range $[f_c - B/2, f_c + B/2]$ and the pulse width T_p , where the pulse width T_p should be no longer than the guard interval T_g in order not to overlap with the OFDM symbol transmission. Therefore, as shown in Fig.2, LFM signal for radar sensing only occupies a very small time portion in part (not all) of OFDM time guards (when there is no OFDM symbol transmission), and this JIAC signalling has almost no influence on the current cellular communication operation and performance.

C. RADAR IMAGING TECHNOLOGY

ISAR is a radar technique that enables the radar imaging functionality for targets, where the radar is stationary and the target is moving relatively. The relative movement of the target contains radial motion and rotation around the central of the target. For the ISAR imaging, the movement of the target creates the synthetic aperture, and the resultant Doppler shift of the target’s scatters from the rotation can be used to generate high resolution radar images. In this work, a typical stationary cellular base station will be modelled as an ISAR system to sense the UAVs.

The transmitted LFM signals can be expressed as

$$s(\hat{t}_f, \hat{t}_m) = P_{tx} G_{tx} \text{rect}\left(\frac{\hat{t}_f}{T_p}\right) \exp\left(j2\pi\left(f_c \hat{t}_f + \frac{1}{2}\gamma \hat{t}_f^2\right)\right) \times \exp(j2\pi f_c \hat{t}_m) \quad (1)$$

$$= P_{tx} G_{tx} s_0(\hat{t}_f) \exp(j2\pi f_c (\hat{t}_f + \hat{t}_m)) \quad (2)$$

where P_{tx} and G_{tx} are the base station transmit power in Watts and antenna gain in linear unit; \hat{t}_f and $\hat{t}_m = mT_r$ are the fast time and slow time, respectively, and $\hat{t}_m + \hat{t}_f$ is the total instantaneous time; $\gamma = B/T_p$ is the frequency linear modulation rate as shown in Fig.3; $s_0(\hat{t}_f) = \text{rect}(\hat{t}_f/T_p) \exp(j\pi\gamma \hat{t}_f^2)$ denotes the basic LFM signal where rect represents the rectangular window function defined as $\text{rect} = 1$ for $|t| \leq 1/2$ and $\text{rect} = 0$ for $|t| > 1/2$.

Considering that the collected echoes is composed of N range bins and M observation echo pulses, when the target has L scatters during the observation, the echo in the m -th pulse can be described as

$$s_e(\hat{t}_f, \hat{t}_m) = \sum_{\ell=1}^L A(\sigma_\ell) s_0(\hat{t}_f - \tau_\ell(\hat{t}_m)) \times \exp(-j4\pi f_c (\hat{t}_f + \hat{t}_m)), \quad (3)$$

where $A(\sigma_\ell)$ denotes the amplitude contributed by the ℓ -th scatter of the flying target to the m -th echo; $d_\ell(\hat{t}_m)$ is the range distance between the radar and the ℓ -th scatter, and $\tau_\ell(\hat{t}_m) = 2d_\ell(\hat{t}_m)/c$ is the caused time delay; and $z(\hat{t}_m)$ denotes the additive while Gaussian noise.

After range compression, 1D HRRPs can be obtained as

$$s_e(\hat{t}_f, \hat{t}_m) = B \sum_{\ell=1}^L A(\sigma_\ell) \text{sinc}(B(\hat{t}_f - 2d_\ell/c)) \times \exp(-j4\pi d_\ell(\hat{t}_m)/\lambda) + z(\hat{t}_m), \quad (4)$$

where $\text{sinc}(B(\hat{t}_f - 2d_\ell/c))$ denotes the envelope of the echo signal with $\text{sinc}(x) = \sin(\pi x)/(\pi x)$; $\exp(-j4\pi d_\ell(\hat{t}_m)/\lambda)$ denotes the phase of the echo signal; $\lambda = c/f_c$ denotes the carrier wavelength.

Assume that the maneuvering target’s movement component - rotation around the rotational centre of the target with a rotational speed is ω and $\Theta = \omega MT_r$ in radian denotes the target’s rotation angle during the observation time MT_r . After range compression, the time difference $\tau_\ell(\hat{t}_m)$ in $\text{sinc}(B(\hat{t}_f - \tau_\ell(\hat{t}_m)))$ reflects the shift in the range bins (rows) that can be compensated by range alignment. After removing the motion phase error, a 2D ISAR high resolution image can be obtained by cross range compression, i.e., doing DFT in the cross range dimension. This autofocus can be realized by joint range compression and cross range compression [31], [32].

III. FEASIBILITY ANALYSIS

This section will provide the feasibility study for the cellular base station imaging. After transmitting the LFM signals from the base station, the signal-to-noise ratio (SNR) of the radar echoes received at the base station can be expressed as follows

$$\text{SNR}_e = \frac{P_{tx} G_{tx} G_{rx} \lambda^2 \sigma}{(4\pi)^3 R^4 (k_B T B) n_f L_s}, \quad (5)$$

where P_{tx} is the base station transmit power in Watts, and G_{tx} , G_{rx} are the base station transmit and receive beamforming gain in linear unit; λ is the carrier wavelength; σ denotes radar cross-section (RCS) of the flying target in square meters, which reflects the echoes; R is the distance/detection range from the base station to the target in meters; k_B , T and B are the Boltzmann constant, the temperature in kelvins, radar sensing spectrum bandwidth in Hertz, thereby the product of $k_B T B$ being the thermal noise; and n_f , L_s denotes the system noise figure, safety margin/loss in the transmission except for the ideal free space path loss.

A. DETECTION RANGE

The received SNR of radar echoes in Eq. (5) implies that the free space path loss is proportional to $1/R^4$, which follows the *inverse fourth-power law* in the detection range R . This is different from the inverse square law for the path loss in communication systems, because the radar echoes experience the round travel that doubles the impact of distance-based path loss compared to the one-way communication transmission.

To guarantee successful target detection, there is usually a minimum SNR threshold requirement for the radar echoes. Given a predefined minimum SNR threshold SNR_0 , the

maximum effective detection range can be derived as

$$R_{max} = \min \left\{ \sqrt[4]{\frac{P_{tx} G_{tx} G_{rx} \sigma \lambda}{(4\pi)^3 \text{SNR}_0 (k_B T B) n_f L_s}}, \frac{c T_r}{2} \right\}, \quad (6)$$

where the term in $\sqrt[4]{\frac{P_{tx} G_{tx} G_{rx} \sigma \lambda}{(4\pi)^3 \text{SNR}_0 (k_B T B) n_f L_s}}$ is derived based on the radar equation (5) and $\text{SNR}_e \geq \text{SNR}_0$. The term $c T_r / 2$ is determined by the pulse repeat interval (PRI) T_r , i.e., the time interval between two adjacent radar pulse, because the next radar pulse should not be sent out before the previous radar pulse returns. To avoid the radar pulse overlapping with the symbol transmission, T_r needs to be set as

$$T_r = n \times (T_s + T_g) \quad (7)$$

where $n \geq 1$ is a positive integer as shown in Fig.2. This determines the pulse repeat frequency of the imaging signals transmission.

The minimum valid detection range can be determined as

$$R_{min} = c T_p / 2, \quad (8)$$

where T_p denotes the radar pulse-width in second, as the typical half-duplex radar cannot receive the echoes when the same pulse has not been transmitted out completely. The reduce of radar pulse width T_p decreases the minimum effective detection range at the cost of less observation time. For the OFDM signal transmission, T_p is up to the guard interval T_g as shown in Fig.2-3.

For the typical 4G LTE OFDM transmission example, the standard symbol duration and the cyclic prefix guard interval are defined as $66.7 \mu s$ and $4.69 \mu s$, respectively, with a carrier spacing of 15 KHz. Without loss of generality, an example of $T_r = 500 \mu s$ and $T_p = 0.4 \mu s$ yields $R_{min} = 60$ meter, and the possible theoretical maximum range $c T_r / 2 = 75$ km will be lower-bounded when consider the SNR requirement SNR_0 in practical as shown in Eq.(6), which will be evaluated later. In theory, the proposed OFDM based LFM signals need to be transmitted for every 70 OFDM guard interval, and only takes a very small portion for the used guard interval, which implies that the above radar imaging signalling strategy nearly does not influence the existing communication OFDM symbols' transmission.

B. IMAGING RESOLUTION

For the ISAR imaging, the range resolution and the cross range resolution refer to the height and width of a pixel in the radar image. Let δ_r and δ_{cr} denote the range resolution and the cross range resolution, respectively, which can be defined as

$$\delta_r = c / 2B, \quad (9)$$

$$\delta_{cr} \approx \lambda / 2\Theta, \quad (10)$$

where Θ is the rotation angle in radian of the flying target during the total observation time, i.e., contributed by the rotation movement component. The higher resolution, the more detailed features of the target will be presented in the radar image. Therefore, high resolution radar imaging is desired.

Based on Eq.(9), the range resolution is enhanced as the bandwidth B increases. From this perspective, radar imaging and wireless communication have the same need - using large bandwidth - to increase the range resolution and the data rate simultaneously. For the cross range resolution in (10), it can be improved as the carrier frequency increases given the fixed rotation angle Θ . Therefore, as the bandwidth is usually limited for the sub-6GHz licensed spectrum, it is preferred to utilize the high frequency, e.g., at unlicensed mm-waves, for high resolution ISAR imaging by benefiting from its small wavelength and large bandwidth. For example, given a typical observed rotation angle of a maneuvering target $\Theta = \pi / 60$, the imaging resolution are $\delta_r = 1.5$, $\delta_{cr} = 1$ meters for a microwave spectrum band $f_c = 3$ GHz, $B = 100$ MHz, and $\delta_r = 0.15$, $\delta_{cr} = 0.1$ meters for a millimetre wave spectrum band $f_c = 30$ GHz, $B = 1$ GHz and, respectively.

C. BEAMFORMING

Given the number of antennas, the narrower beam generated will provide the higher beam gain G_{tx} and G_{rx} in Eq.(5). Without loss of generality, when N_a base station antennas are used in transmitting and receiving, the peak phased-only beamforming gain can be roughly characterized as $G_{tx} = G_{rx} \approx N_a^2$ in linear unit. Therefore, the large scale antenna array, e.g., massive MIMO, is also desired in radar sensing by benefiting the higher beamforming gain to combat the inverse fourth-power law based path loss of radar echoes.

D. TRADE-OFFS

As we analysed above, large bandwidth B is desired to achieve high range resolution δ_r , while the large B also introduce the high thermal noise power $k_B T B$ that degrades the received SNR of echoes. On the other hand, high carrier frequency along with the large bandwidth, e.g., mm-wave, is expected to increase both the range resolution and cross range resolution. However, the high carrier frequency transmission suffers from more severe free space path loss, which will limit the effective detection range.

In the typical cellular mobile communication networks, different carrier frequencies usually correspond different frequency bandwidth, e.g., the unlicensed mm-wave allows larger transmission bandwidth than the sub-3G Hz microwave. For instance, 5G NR FR1 band n1 has $f_c = 2100$ MHz and $B = 5 - 50$ MHz but 5G NR FR2 band n259 corresponds to $f_c = 41$ GHz and $B = 50 - 400$ MHz, respectively. Therefore, the choice of f_c and B are related with each other. There exists a trade-off to determine suitable (f_c, B) according to the needs to jointly balance the imaging resolution, path loss, noise power, and the detection range.

In terms of the implementation and complexity, the Nyquist theorem states that a signal with the bandwidth B can be completely reconstructed if $2B$ samples per second are used. Therefore, the radar echoes' sampling data is increasing with the frequency bandwidth B , which causes a higher demanding for the data storage and processing capability at the cellular base station. Especially, when the higher

TABLE 1. Cellular base station imaging performance.

Carrier frequency	3G/4G (≤ 3 GHz)	5G FR1 (3 – 6 GHz)	5G FR2 (mm-wave)
Bandwidth	5-100 MHz	5-400 MHz	up to 2 GHz
Range resolution	30 - 1.5 meter	30 - 0.35 meter	up to 0.075 meter
Cross range resolution (for $\Theta = \pi/36$)	1.91 meter@900MHz, 0.96 meter@1800MHz	0.49 meter@3.5GHz	0.06 meter@28GHz
Radar sensing	detection (HRRP)	small targets: detection (HRRP) large targets: 2D imaging	2D imaging

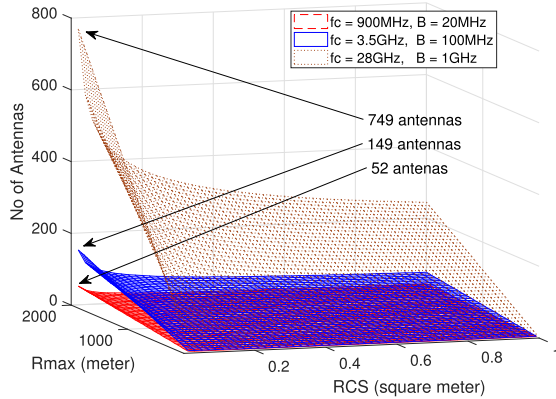


FIGURE 4. The minimum number of antennas required varying with target's RCS and maximum detection range.

resolution imaging is expected, the larger frequency bandwidth is needed, as defined in Eq. (9). In this case, the high resolution imaging quality might be conflicting with data storage and processing capability of the cellular base station. This trade-off can be balanced according to the hardware capacity of the cellular base station.

E. NUMERICAL FEASIBILITY STUDY

To evaluate the feasibility of cellular base station imaging, we consider three typical types of cellular base stations: 1) 3G/4G base station with $f_c = 900MHz$, $B = 20MHz$, 2) 5G base station with FR1 $f_c = 3.5GHz$, $B = 100MHz$, and 3) mm-wave base station $f_c = 28GHz$, $B = 1GHz$. Consider the typical base station transmit power $P_{tx} = 43 dBm$, noise figure $n_f = 5 dB$ and the safety margin/loss $L_s = 3 dB$. Given a minimum required SNR $SNR_0 = 10 dB$, the simulation is to estimate how many antennas at least are needed to detect the target with the varying RCS from 0.01 to 1 square meter and the range from 100 to 2000 meters.

Fig.4 illustrates numerical results based on the above system setting. It is observed that the number of required antennas is increasing with the detection range R_{max} to combat the increasing path loss, but decreasing with the target RCS. Note that $N_a = 52, 149$ and 749 antennas are needed for the 3G/4G base station imaging operating at $f_c = 900MHz$, 5G base station at $f_c = 3.5GHz$ and mm-wave base station at $f_c = 28GHz$, respectively, to detect a 2000 meters away target with a very small RCS of 0.01 square meter. It is worth to know that a flying bird has a RCS as small as

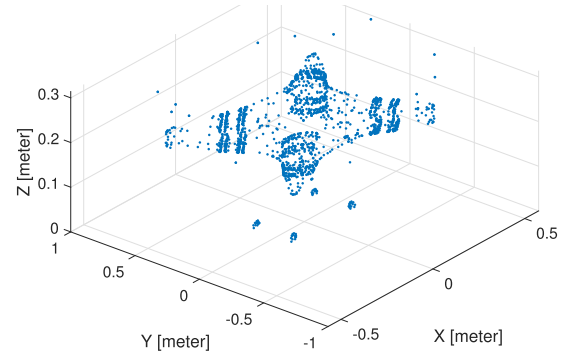


FIGURE 5. 3D scattering model for a typical four-rotor drone.

0.01 square meter. Even these number of antennas might be feasible for the corresponding cellular base stations. When low-and-middle altitude UAVs with the reasonable sizes are considered, the required number of antennas can be greatly reduced for the RCS that is larger than 0.01 square meter and reasonable range, e.g., hundreds of meters. Therefore, based on this simulation, it is feasible to realize cellular base stations imaging for UAVs.

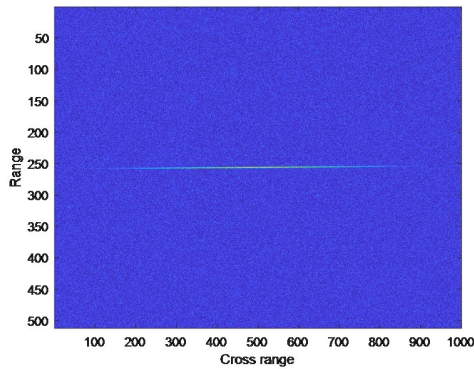
The table 1 summarizes the key observation and suggestions for the capability of cellular base station imaging.

IV. UAV IMAGING ILLUSTRATION

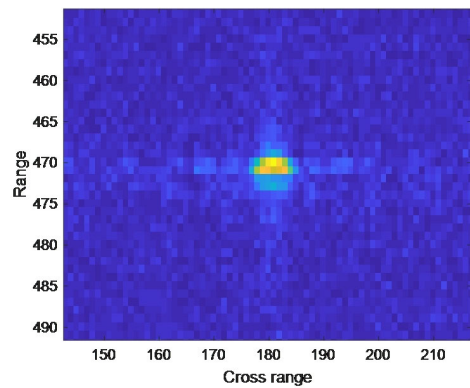
In this section, cellular base station imaging is illustrated by processing the collected 1000 echoes with the pulse width $T_p = 0.4\mu s$ and PRI $T_r = 500\mu s$, thereby the total radar observation time 0.5 s. Assume that the maneuvering target has a typical rotation angle of $\Theta = \pi/36$ during the observation time block. A four-rotor drone is used to model flying targets with different size and its basic 3D scattering model is given in Fig.5. In the simulation, we scale the same drone model in Fig.5 to denote the different sized UAVs in order to do a fair performance comparison for the imaging capability with different base station settings.

A. SIMULATION RESULTS FOR 900MHz

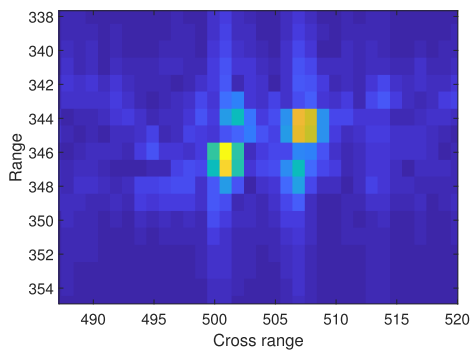
This section is to firstly evaluate the base station operating at the carrier frequency 900MHz with bandwidth $B = 20MHz$. Fig.6a illustrates the 1000 echoes after range compression, from which we can see that there is a very narrow "bright line" that is formed by the peaks of 1000 compressed echo (HRRPs). After range alignment and cross range compression, the 2D image is generated as shown in Fig.6b, which



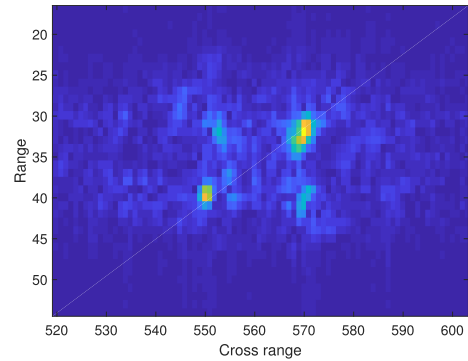
(a) Range compression: 16 antennas, target size $0.8m \times 1m$ ($RCS \delta = 0.33m^2$) and distance 1000m



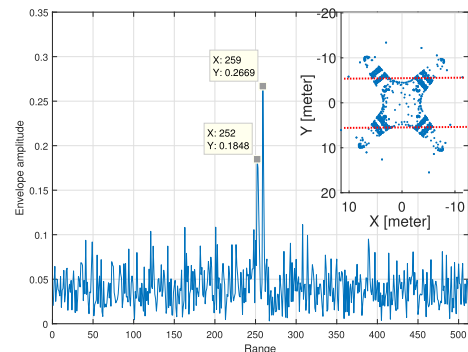
(b) 2D image: 16 antennas, target size $0.8m \times 1m$ ($RCS \delta = 0.33m^2$) and distance 1000m



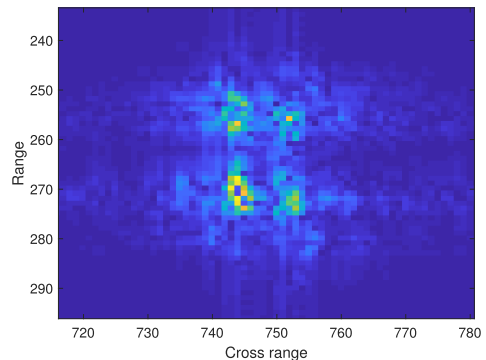
(c) 2D image: 32 antennas, target size $24m \times 30m$ and distance 2000m



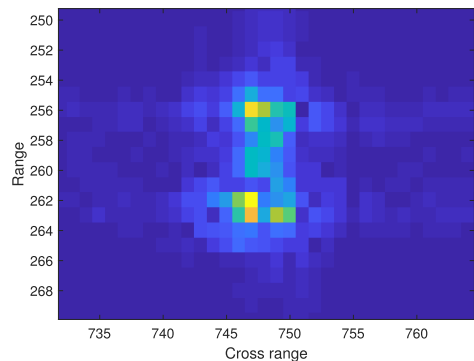
(a) 2D image: target size $16m \times 20m$ and distance 1000m



(b) HRRP: target size $16m \times 20m$ and distance 3000m



(c) 2D image: target size $8m \times 10m$ and distance 200m



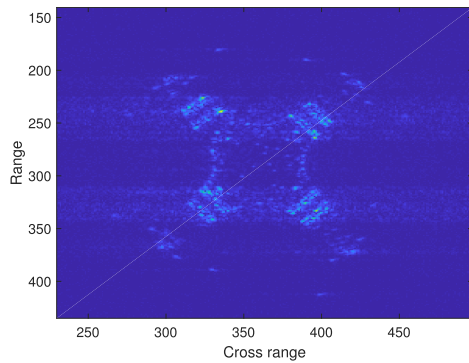
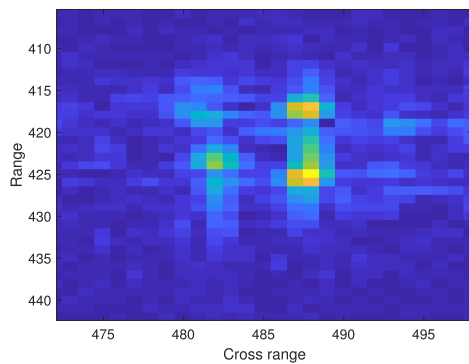
(d) 2D image: target size $2.4m \times 3m$ and distance 200m

FIGURE 6. Base station imaging examples for 900 MHz band.

has only one focused peak. This is because the drone in size of $0.8m \times 1m$ is smaller or comparable to the low range resolution $\delta_r = 7.5m$ and the cross range resolution $\delta_{cr} = 0.955m$ so that the target takes only one pixel and its side lobes may also take a few pixels. In this case, the size and the shape of the target cannot be recognised but can be only detected. When the large target is considered, e.g., the drone is scaled up to $24m \times 30m$, it can be imaged as Fig.6c, from which the shape of the four-rotor drone can be roughly observed, and also we can roughly estimate the size of the drone by counting the number of range bins and the number of columns. Therefore,

FIGURE 7. 64-antenna base station imaging examples for 3.5GHz band.

the low frequency below $3GHz$ is more suitable for the long range detection, except for the very large-sized targets.

(a) 2D image: drone size $8m \times 10m$ and distance $200m$ (b) 2D image: drone size $0.8m \times 1m$ and distance $200m$ **FIGURE 8.** 512-antenna base station imaging examples for 28GHz band.

B. SIMULATION RESULTS FOR 3.5GHz

In this part, we firstly consider a 64-antenna 5G base station operating at the carrier frequency $3.5GHz$ and $B = 100MHz$. Consider a large target in the size of $16m \times 20m$, Fig.7a shows the 2D radar image for the drone with the distance $1000m$ from the base station. In this case, with the range resolution $\delta_r = 1.5m$ and the cross range resolution $\delta_{cr} = 0.49m$, the shape of the drone is roughly shown. When we increase the distance to $3000m$, the target cannot be imaged in two dimensions due to low SNR caused by the severe path loss. Yet, the HRRP can be still obtained as Fig.7b, from which the range size of the target can still be roughly estimated by accounting how many range bins the target reflected peaks take.

When the bandwidth is increased to $B = 400MHz$ by using carrier aggregation, it might be allowed to image smaller sized target. For example, Fig.7c clearly show the target in size of $8m \times 10m$ by benefiting from the high range resolution $\delta_r = 0.375m$ and the cross range resolution $\delta_{cr} = 0.4911m$. However, when the size of the target is further reduced to $2.4m \times 3m$, the width of the drone ($3m$) only takes a few cross range pixels so that the target cannot be clearly presented in cross range as shown in Fig.7d. Therefore, the 5G base station at $3.5GHz$ is more suitable to perform 2D imaging for the middle-and-large sized targets at middle-and-long range.

C. SIMULATION RESULTS FOR 28GHz

This part shows the imaging performance for the 512-antenna base station operating at the carrier frequency of $28GHz$.

For the bandwidth is $B = 2GHz$ at $28GHz$, very high imaging resolution can be achieved - the range resolution $\delta_r = 0.075m$ and the cross range resolution $\delta_{cr} = 0.0614m$. Therefore, the shape and even detailed features of the target with size of $8m \times 10m$ and a $200m$ distance are clearly presented as the imaging example in Fig.8a. When the target size is reduced to the very small size $0.8m \times 1m$, it is still feasible to observe the shape and estimate the size of this very small target, as shown in Fig.8b. However, the path loss at mm-wave becomes much more severe compared with the sub-6GHz microwave, which usually results in low SNR for the far away targets. Therefore, the mm-wave band is more suitable to achieve very high resolution imaging for short-range and small-sized targets due to its very high resolution and severe path loss.

V. CONCLUSION

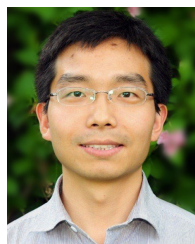
In this work, we systematically study and illustrated the concept of cellular base station imaging, along with its signalling strategy and imaging mechanism. The feasibility study provides a theoretical view and analysis of this JIAC idea. Note that this JIAC method requires a very little change of the current OFDM transmission in cellular mobile networks, and has almost no influence on the current communication operation and performance. Therefore, this cellular base station imaging has a great potential for the practical application. In terms of implementation, high resolution imaging needs wide frequency band, but it in return will cause large radar echoes' sampling data, resulting in a high hardware demanding of the radar data storage and processing capability at a cellular base station.

It is for the first time to illustrate the proposed cellular base station imaging concept numerically, from which the imaging performance where evaluated for the different types of cellular base stations, for example at $900MHz$, $3.5GHz$ and $28GHz$, respectively. The results imply that cellular base station at sub- $3GHz$ is more suitable for the long-range target detection due to its low range resolution and less severe path loss. In contrast, mm-wave bands allows the base station to "see" the detailed features of targets but at short distance because of its severe path loss and very high range resolution. The frequency range at $3.5GHz$ can be a trade-off choice, especially when the bandwidth becomes large by using carrier aggregation.

REFERENCES

- [1] H. Shakhatreh, A. H. Sawalmeh, A. Al-Fuqaha, Z. Dou, E. Almaita, I. Khalil, N. S. Othman, A. Khreishah, and M. Guizani, "Unmanned aerial vehicles (UAVs): A survey on civil applications and key research challenges," *IEEE Access*, vol. 7, pp. 48572–48634, 2019.
- [2] B. Alzahrani, O. S. Oubbati, A. Barnawi, M. Atiquzzaman, and D. Alghazzawi, "UAV assistance paradigm: State-of-the-art in applications and challenges," *J. Netw. Comput. Appl.*, vol. 166, Sep. 2020, Art. no. 102706.
- [3] O. S. Oubbati, M. Atiquzzaman, T. Ahamed Ahanger, and A. Ibrahim, "Softwarization of UAV networks: A survey of applications and future trends," *IEEE Access*, vol. 8, pp. 98073–98125, 2020.
- [4] A. Ghosh, A. Maeder, M. Baker, and D. Chandramouli, "5G evolution: A view on 5G cellular technology beyond 3GPP release 15," *IEEE Access*, vol. 7, pp. 127639–127651, 2019.

- [5] D. Solomitskii, M. Gapeyenko, V. Semkin, S. Andreev, and Y. Koucheryavy, "Technologies for efficient amateur drone detection in 5G millimeter-wave cellular infrastructure," *IEEE Commun. Mag.*, vol. 56, no. 1, pp. 43–50, Jan. 2018.
- [6] P. Kumari, J. Choi, N. Gonzalez-Prelcic, and R. W. Heath, Jr., "IEEE 802.11ad-based radar: An approach to joint vehicular communication-radar system," *IEEE Trans. Veh. Technol.*, vol. 67, no. 4, pp. 3012–3027, Apr. 2018.
- [7] A. R. Chiriyath, B. Paul, and D. W. Bliss, "Radar-communications convergence: Coexistence, cooperation, and co-design," *IEEE Trans. Cogn. Commun. Netw.*, vol. 3, no. 1, pp. 1–12, Mar. 2017.
- [8] T. Wild, V. Braun, and H. Viswanathan, "Joint design of communication and sensing for beyond 5G and 6G systems," *IEEE Access*, vol. 9, pp. 30845–30857, 2021.
- [9] *European Vision for the 6G Network Ecosystem*, 5G Infrastructure Association, Brussels, Belgium, 2021.
- [10] B. Paul, A. R. Chiriyath, and D. W. Bliss, "Survey of RF communications and sensing convergence research," *IEEE Access*, vol. 5, pp. 252–270, 2016.
- [11] J. A. Zhang, M. L. Rahman, K. Wu, X. Huang, Y. J. Guo, S. Chen, and J. Yuan, "Enabling joint communication and radar sensing in mobile networks—A survey," *IEEE Commun. Surveys Tuts.*, early access, Oct. 25, 2021, doi: [10.1109/COMST.2021.3122519](https://doi.org/10.1109/COMST.2021.3122519).
- [12] M. L. Rahman, J. A. Zhang, X. Huang, Y. J. Guo, and R. W. Heath, "Framework for a perceptive mobile network using joint communication and radar sensing," *IEEE Trans. Aerosp. Electron. Syst.*, vol. 56, no. 3, pp. 1926–1941, Jun. 2020.
- [13] A. Hassani, M. G. Amin, Y. D. Zhang, and F. Ahmad, "Signaling strategies for dual-function radar communications: An overview," *IEEE Aerosp. Electron. Syst. Mag.*, vol. 31, no. 10, pp. 36–45, Oct. 2016.
- [14] F. Liu, C. Masouros, A. P. Petropulu, H. Griffiths, and L. Hanzo, "Joint radar and communication design: Applications, state-of-the-art, and the road ahead," *IEEE Trans. Commun.*, vol. 68, no. 6, pp. 3834–3862, Jun. 2020.
- [15] T. Huang, N. Shlezinger, X. Xu, Y. Liu, and Y. C. Eldar, "MAJoRCOM: A dual-function radar communication system using index modulation," *IEEE Trans. Signal Process.*, vol. 68, pp. 3423–3438, 2020.
- [16] C. Sturm and W. Wiesbeck, "Waveform design and signal processing aspects for fusion of wireless communications and radar sensing," *Proc. IEEE*, vol. 99, no. 7, pp. 1236–1259, Jul. 2011.
- [17] P. Kumari, S. A. Vorobyov, and R. W. Heath, "Adaptive virtual waveform design for millimeter-wave joint communication–Radar," *IEEE Trans. Signal Process.*, vol. 68, pp. 715–730, 2020.
- [18] Y. Liu, G. Liao, J. Xu, Z. Yang, and Y. Zhang, "Adaptive OFDM integrated radar and communications waveform design based on information theory," *IEEE Commun. Lett.*, vol. 21, no. 10, pp. 2174–2177, Oct. 2017.
- [19] F. Liu, C. Masouros, T. Ratnarajah, and A. Petropulu, "On range sidelobe reduction for dual-functional radar-communication waveforms," *IEEE Wireless Commun. Lett.*, vol. 9, no. 9, pp. 1572–1576, Sep. 2020.
- [20] C. B. Barneto, T. Riihonen, M. Turunen, L. Anttila, M. Fleischer, K. Stadius, J. Ryynanen, and M. Valkama, "Full-duplex OFDM radar with LTE and 5G NR waveforms: Challenges, solutions, and measurements," *IEEE Trans. Microw. Theory Techn.*, vol. 67, no. 10, pp. 4042–4054, Oct. 2019.
- [21] W. Yuan, F. Liu, C. Masouros, J. Yuan, D. W. K. Ng, and N. Gonzalez-Prelcic, "Bayesian predictive beamforming for vehicular networks: A low-overhead joint radar-communication approach," *IEEE Trans. Wireless Commun.*, vol. 20, no. 3, pp. 1442–1456, Mar. 2021.
- [22] C. Shi, F. Wang, S. Salous, and J. Zhou, "Joint subcarrier assignment and power allocation strategy for integrated radar and communications system based on power minimization," *IEEE Sensors J.*, vol. 19, no. 23, pp. 11167–11179, Dec. 2019.
- [23] F. Liu, C. Masouros, A. Li, H. Sun, and L. Hanzo, "MU-MIMO communications with MIMO radar: From co-existence to joint transmission," *IEEE Trans. Wireless Commun.*, vol. 17, no. 4, pp. 2755–2770, Apr. 2018.
- [24] Y. Zhuang, L. Hua, L. Qi, J. Yang, P. Cao, Y. Cao, Y. Wu, J. Thompson, and H. Haas, "A survey of positioning systems using visible LED lights," *IEEE Commun. Surveys Tuts.*, vol. 20, no. 3, pp. 1963–1988, 3rd Quart., 2018.
- [25] Y. Zhuang, Q. Wang, M. Shi, P. Cao, L. Qi, and J. Yang, "Low-power centimeter-level localization for indoor mobile robots based on ensemble Kalman smoother using received signal strength," *IEEE Internet Things J.*, vol. 6, no. 4, pp. 6513–6522, Aug. 2019.
- [26] C. Chen, Y. Chen, H.-Q. Lai, Y. Han, and K. J. R. Liu, "High accuracy indoor localization: A WiFi-based approach," in *Proc. IEEE Int. Conf. Acoust., Speech Signal Process. (ICASSP)*, Mar. 2016, pp. 6245–6249.
- [27] Q. Chen, B. Tan, K. Woodbridge, and K. Chetty, "Indoor target tracking using high Doppler resolution passive Wi-Fi radar," in *Proc. IEEE Int. Conf. Acoust., Speech Signal Process. (ICASSP)*, Apr. 2015, pp. 5565–5569.
- [28] F. Adib and D. Katabi, "See through walls with WiFi!" in *Proc. ACM SIGCOMM Conf. (SIGCOMM)*, Aug. 2013, pp. 75–86.
- [29] D. Huang, R. Nandakumar, and S. Gollakota, "Feasibility and limits of Wi-Fi imaging," in *Proc. 12th ACM Conf. Embedded Netw. Sensor Syst.*, Nov. 2014, pp. 266–279.
- [30] H. Li, "Imaging using millimeter wave communication networks: A bonus SAR," 2020, *arXiv:2011.08801*.
- [31] B. Zheng, S. Changyin, and X. Mengdao, "Principles and algorithms for inverse synthetic aperture radar imaging of manoeuvring targets," in *Proc. Rec. IEEE Int. Radar Conf.*, May 2000, pp. 316–321.
- [32] P. Cao, M. Xing, G. Sun, Y. Li, and Z. Bao, "Minimum entropy via subspace for ISAR autofocus," *IEEE Geosci. Remote Sens. Lett.*, vol. 7, no. 1, pp. 205–209, Jan. 2010.



PAN CAO received the B.Eng. and M.Eng. degrees from Xidian University, China, in 2008 and 2011, respectively, and the Dr.-Ing. (Ph.D.) degree in electrical engineering from TU Dresden, Germany, in 2015.

He worked on SAR/ISAR imaging and signal processing at the National Laboratory of Radar Signal Processing, Xidian University, from 2008 to 2010. He was a Postdoctoral Research Associate working on an EPSRC 5G project with the University of Edinburgh, from 2015 to 2017, and a Visiting Researcher at Princeton University, in 2017. He has been a Senior Lecturer in electronics and communications with the University of Hertfordshire, U.K., since 2017. His current research interests mainly include millimeter-wave communication, antenna array signal processing, and the integration of radar sensing and communication. He received the Best Paper Awards of IEEE SPAWC 2012 and International Conference on Machine Learning and Networking 2018 and the Qualcomm Innovation Fellowship Award (QInF), in 2013. He is the Vice-Chair of the Special Interest Group on the integration of sensing and communication in IEEE ComSoc's Radio Communications Committee. He currently serves as an Associate Editor for the *EURASIP Journal on Wireless Communications and Networking*.

...